Three major dimensions of human brain cortical ageing in relation to cognitive decline across the 8th decade of life.

Cox, SR✉[1,2,3], Harris MA[4], Ritchie SJ[5], Buchanan CR[1,2,3], Maria Valdés Hernández[1,3,7], Janie Corley[1,2], Adele M Taylor[1,2], Madole JW[6], Harris SE[1,2], Whalley HC[4], McIntosh AM[4], Russ TC[1,4,7,8], Bastin ME[1,3,7], Wardlaw JM[1,3,7], Deary IJ[1,2]*, Tucker-Drob EM[6]*.

[1] *Lothian Birth Cohorts group, The University of Edinburgh, UK,*

[2] *Department of Psychology, The University of Edinburgh, UK,*

[3] *Scottish Imaging Network, A Platform for Scientific Excellence (SINAPSE) Collaboration, Edinburgh, UK,*

[4] *Division of Psychiatry, The University of Edinburgh, UK,*

[5] *Social, Genetic and Developmental Psychiatry Centre, King's College London, London, UK,*

[6] *Department of Psychology, University of Texas, Austin, Texas, USA,*

[7] *Centre for Clinical Brain Sciences, The University of Edinburgh, UK.*

* *authors contributed equally*

✉corresponding author: Simon R. Cox, Lothian Birth Cohorts group, Department of Psychology, The University of Edinburgh, Edinburgh EH8 9JZ, UK. Email: simon.cox@ed.ac.uk.

Conflicts of Interest: None.

Abstract

Different brain regions can be grouped together, based on cross-sectional correlations among their cortical characteristics; this patterning has been used to make inferences about ageing processes. However, cross-sectional brain data conflates information on ageing with patterns that are present throughout life. We characterised brain cortical ageing across the 8th decade of life in a longitudinal ageing cohort, at ages ~73, ~76, and ~79 years, with a total of 1,376 MRI scans. Volumetric *changes* among cortical regions of interest (ROIs) were more strongly correlated (average $r = 0.805$, SD = 0.252) than were *cross-sectional* volumes of the same ROIs (average $r = 0.350$, SD = 0.178). We identified a broad, cortex-wide, dimension of atrophy that explained 66% of the variance in longitudinal changes across the cortex. Our modelling also discovered more specific fronto-temporal and occipito-parietal dimensions, that were orthogonal to the general factor and together explained an additional 20% of the variance. The general factor was associated with declines in general cognitive ability ($r = 0.430$, $p < 0.001$) and in the domains of processing speed ($r = 0.383$, $p < 0.001$) and memory ($r = 0.372$, $p < 0.001$), but not with visuospatial ability ($r = 0.143$, $p = 0.151$). Individual differences in brain cortical atrophy with ageing are manifest across three broad dimensions of the cerebral cortex, the most general of which is linked with declines in both processing speed and memory. Longitudinal approaches will prove invaluable for distinguishing lifelong patterns of brain-behaviour associations from patterns that are specific to aging.

Introduction

Accurately characterising patterns of brain ageing, alongside their determinants and functional significance, is a major challenge for developmental neuroscience. The eighth decade of life is a time in which risk for cognitive decline and dementia begins to accelerate markedly (Prince et al., 2014), alongside consequent increases in personal and societal burden, and poorer quality of life (Fineberg et al., 2013, Wimo et al., 2013; Bárrios et al., 2013). The general under-representation of participants aged over 70 years in life-course brain imaging studies has been a problem for this research, along with the fact that many of our inferences about the progression of ageing-related brain changes come from cross-sectional datasets. Whereas cross-sectional information can potentially be informative for ageing, it has been strongly criticised in some quarters since it—unlike analysis of longitudinal data—is unable adequately to approximate the dimensionality and time-dependent dynamics of ageing (Raz & Lindenberger, 2011, Salthouse, 2011; Fjell et al., 2012). Here, we investigate individual differences in patterns of cortical ageing using longitudinal data in a large sample of generally-healthy community-dwelling adults who were brain scanned three times, from their early-to-late 70s.

Older age is accompanied by a general decline in overall cerebral volume, with corresponding ventricular enlargement and increasing aggregation of other features such as white matter hyperintensites, and alterations in white matter microstructural properties (Fjell & Walhovd, 2010; Cox et al., 2016; Wardlaw et al., 2015). At the more fine-grained regional level, cortical ageing is not uniform. Age effects appear to be stronger for some regions than others, with those areas ontogenetically and phylogenetically latest to develop—those that are more strongly linked to more complex cognitive functions—being those most affected (see Fjell et al., 2014). However, it has become increasingly apparent that univariate accounts of brain ageing (considering a single brain area in isolation) are suboptimal for accurately characterising patterns of brain ageing. More recent accounts of brain organisation have used cross-sectional data to identify clusters of regions with shared morphometric characteristics (Doucet et al., 2018; Doan et al., 2017; Hafkemeijer et al., 2014; Douaud et al., 2014; Smith et al. ,2019). Whereas such accounts have the potential to capture the coordinated patterns of age-related atrophy in health and disease, they are predominantly based on cross-sectional data, which, as noted above, cannot fully reflect the dynamics of within-individual change (Molenaar, 2004). As such, the network configuration described by regional (cross-sectional) structural correlations is not necessarily optimal for evaluating brain ageing and its correlates.

Discovering the patterning of longitudinal changes in brain structure, and how such changes relate to longitudinal ageing-related cognitive decline, is crucial to understanding the neurobiology of cognitive ageing as distinct from the neurobiology of lifelong levels of cognitive function. Put simply, the fact that aspects of brain regions' structure *correlate* together when measured on one occasion does not mean that they necessarily *change* together over time. Using longitudinal data to uncover the degree to which individuals show distinct patterns of cortical atrophy is likely to be valuable in the stratification of

ageing subtypes against current and future cognitive and health outcomes, other biomarkers, and their potentially distinct determinants.

We are aware of only one previous study of multivariate longitudinal changes in cortical structure, which was conducted in an age-heterogeneous sample of participants with amnestic mild cognitive impairment (aMCI; Carmichael et al., 2013, N = 317). That study identified five groupings, each of which comprised regions with strongly correlated atrophic profiles. These broadly described 1) posterior default mode, 2) prefrontal, 3) medial temporal, 4) 'spared' (sensorimotor and occipital), and 5) a diffuse global atrophic pattern. The authors concluded that this might reflect multiple patterns of coordinated neuronal degradation with potentially distinct biological substrates (Carmichael et al., 2013). As yet, it remains unclear whether the presence of cross-sectional correlations between brain regions bears any relation to their shared patterns of change over time among non-clinical, generally-healthy older adults, whose neurobiological and cognitive changes may occur during early, prodromal phases of cognitive decline, when prevention and intervention efforts may be most likely to succeed.

In the present study, we used longitudinal data collected on three occasions across the eighth decade of life to characterise the patterns of cortical ageing in a group of community-dwelling older adults. We first estimated the cross-sectional levels (baselines) and longitudinal changes for each cortical region. We then explored their factor structure to discover any clusters of regions that exhibited correlated changes over time. We next related the factors of brain cortical change to changes in major age-sensitive domains of cognitive capability: memory, visuo-spatial reasoning, and processing speed. We placed particular emphasis on documenting how factors underlying cortex-wide and more regionally-specific constellations of variation in volumetric atrophy related to longitudinal ageing-related cognitive declines.

Methods

Participants

Participants were drawn from the Lothian Birth Cohort 1936 (LBC1936; Deary et al., 2012; Taylor et al., 2018; Corley et al., 2018), a longitudinal study of brain and cognitive ageing in healthy community-dwelling older adults. The participants were initially recruited into this same-year-of-birth project at around 70 years of age (Wave 1, N = 1,091) where they underwent a number of cognitive, health and medical assessments. They were subsequently followed-up at ages ~73 (Wave 2, N = 866), ~76 (Wave 3, N = 697), and ~79 (Wave 4, N = 550), where they completed mostly the same tests as previously, with the addition of structural brain imaging assessments (see next section). Here, we included participants for Waves 2, 3 and 4, for whom concomitant brain imaging and cognitive data were available. Whole blood was drawn at baseline from which genomic DNA was isolated (at the Wellcome Trust Clinical Research Facility Genetics Core, Western General Hospital, Edinburgh). Participants provided written informed consent prior to testing at each wave. The LBC1936 study was

approved by the Multi-Centre for Scotland (MREC/01/0/56), Lothian (LREC/2003/2/29) and Scotland A (07/MRE00/58) Research Ethics Committees.

MRI Acquisition & Analysis

Brain structural MRI data were acquired according to a previously published protocol (Wardlaw et al., 2011) at Waves 2, 3 and 4. A 1.5T GE Signa HDxt clinical scanner (General Electric, Milwaukee, WI, USA) with a manufacturer-supplied eight-channel phased-array head coil was used to acquire 3D T1-weighted volumes in the coronal orientation at 1mm isotropic resolution. All scans were assessed by a consultant neuroradiologist, which included assessment of evidence for stroke. Acquired volumes were then processed in FreeSurfer v5.1 (Dale et al., 1999; Fischl et al., 1999; Fischl et al., 2004). This involved segmentation of each volume, identifying brain tissue types, followed by parcellation of cortical grey matter into 34 regions per hemisphere, according to the Desikan-Killiany atlas (Desikan et al., 2006; Supplementary Figure 1). Output for each image was visually assessed for segmentation and parcellation errors, which were then corrected manually. Segmentations with errors that could not be corrected were excluded. Using FreeSurfer's longitudinal processing stream (Reuter et al., 2012), each participant's data across all waves were then resampled together, in order to minimise any erroneous longitudinal variation in parcellation. Regional volumes for each participant at each wave were then derived from the output of the longitudinal stream. The following analyses are based on 1,376 MRI scans (Wave 2 N = 629; Wave 3 N = 428; Wave 4 N = 319).

Cognitive Measurement

Participants underwent a detailed battery of standardised cognitive tests that assessed major domains relevant to ageing. These were categorised into three cognitive domains based upon well-fitting, hierarchical structural equation models tested in our previously-published work (Tucker-Drob et al., 2014; Ritchie et al., 2016). Visuospatial ability was indicated by performance on Matrix Reasoning and Block Design from the Wechsler Adult Intelligence Scale III^{UK} (WAIS III^{UK}; Wechsler, 1998a), and Spatial Span Forward and Backward from the Wechsler Memory Scale III^{UK} (WMS III^{UK}; Wechsler, 1998b). Processing Speed was measured with Symbol Search and Digit Symbol Substitution from the WAIS III^{UK}, Visual Inspection Time (Deary et al., 2004), and Four-Choice Reaction Time (Deary et al., 2001). Verbal Memory ability was ascertained using Logical Memory (sum of immediate and delayed) and Verbal Paired Associates (sum of immediate and delayed) from the WMS III^{UK}, and Digit Span Backwards from the WAIS III^{UK}. The Mini-Mental State Examination (MMSE; Folstein et al., 1975) was also administered.

APOE Genotyping

TaqMan technology was used to identify *APOE* e4 carriers. Status was determined according to genotyping on the two polymorphic sites (rs7412 and rs429358) that account for e2, e3 and e4 alleles (Wenham et al., 1991).

Statistical Analysis

Figure 1 illustrates the analytical framework. First, we characterised the trajectories of cortical ageing at the level of each the 34 brain regions of interest (ROI). For each ROI per hemisphere, we fitted a separate growth curve in a structural equation modelling (SEM) framework in R (R Core Team) using the 'lavaan' package (Roseel, 2012). We used full information maximum likelihood estimation throughout. The unstandardized estimate of slope was reported as % change per annum.

To investigate the possibility that there are spatially distinct dimensions of cortical ageing, our first step was to run an exploratory factor analysis (EFA) on the intercepts and slopes of the left hemisphere brain cortical ROIs (to be subsequently tested against the right hemisphere in a pseudo-replication). First, we fitted a SEM in which growth curves (intercepts and slopes) for all 34 left hemisphere ROIs were freely estimated. We then extracted the estimated latent correlation matrix and separated it into two parts; one of intercepts and one of slopes. The 'nearPD' function (from the 'psych' package in R; Revelle, 2015) was used to scale estimated values so that they were positive definite (ranging from -1 to 1, due to some residual variances initially having negative estimates).

Slope and intercept covariances were examined as hierarchically-clustered heatmaps. Based on this information, we conducted a Schmid-Leiman (Schmid & Leiman, 1957) transformation (from the 'psych' package) to examine the oblique factor structure beyond any common variance shared (i.e. a bi-factor model). This transformation was conducted separately for intercepts and slopes, retaining factor loadings >0.3. To test whether the identified correlation structure for intercepts and slopes was replicable (age differences in brain structural measures are extremely modest-to-null according to cross-sectional estimates; Takao et al., 2010; Cox et al., 2016; Kong et al., 2018), we then repeated this exploratory analysis for the right hemisphere ROIs. We used Pearson's *r* and the coefficient of factor congruence (Burt, 1948) to formally quantify whether the resultant factor loading pattern replicated across hemispheres. We also ran these same two comparisons between the factor structure of intercepts and slopes within each hemisphere; that is, we tested whether brain cortical *level* correlations resembled cortical *change* correlations.

Although all participants were free from dementia diagnosis at baseline recruitment, we conducted a sensitivity analysis to ascertain whether the observed correlational structure may have been driven by participants who may have subsequently developed dementia or cognitive impairment. We did so by removing all those who had either, i) subsequently reported having received a diagnosis of dementia at any wave, or ii) had a score <24 on the MMSE at any wave. We then compared the resultant loading patterns with the results from

the whole group analysis, using Pearson's *r* and the coefficient of factor congruence, as above. We conducted a second sensitivity analysis, repeating these steps, this time removing participants whose MRI scans indicated stroke, as assessed by a consultant neuroradiologist (author JMW).

Next, we conducted a confirmatory factor analysis, imposing the slope factor structure identified from the Schmid-Leiman transform. That is, we used the Schmid-Leiman loadings as starting values to estimate the loadings of each ROI's slope factor on the relevant slope factor of cortical change. Given that the EFA was conducted on correlation matrices rather than a data frame itself, this step was necessary to allow us to investigate correlates of the observed factors of change. Growth curve intercepts for each ROI were freely-estimated, and allowed to correlate with all other latent variables. Where the loadings of any ROI slope onto any slope factor were non-significant ($p < 0.05$), these were set to zero.

We then extended these multivariate SEMs to analyse the degree to which the factors of cortical change were associated with trajectories of cognitive change. We examined associations at the level of general cognitive ability ('*g*'; see Supplementary Figure 2 and Deary et al., 2010), and for the correlated cognitive domains of visuospatial, processing speed and memory, as well as with *APOE* e4 allele carrier status. The levels and changes in cognitive function were estimated in a Factor of Curves growth curve SEM (whereby each cognitive test over time has its own intercept and slope, and these contribute to an overall latent intercept and slope of all cognitive tests in that domain; McArdle, 2009). We fitted one model for each of the cognitive analyses (*g*, visuospatial, processing speed, memory) in association with our model of cortical change. To aid model convergence and ensure construct consistency, we fixed factor loadings for both the cognitive and MRI sides of the SEM according to our initial measurement models / confirmatory factor analyses (CFAs). Specifically, for the brain cortical aspects of these models, we fixed the ROI slope factor loadings on the three overall slope factors. For each of the four cognitive models (three cognitive domains and overall general cognitive model), we fixed the factor loadings of the cognitive test latent intercept and latent slope factors on the cognitive domain intercept and slope factors. The cognitive test intercepts and slopes were corrected for sex; the CFA of cortical change indicated that there were no sex differences in any cortical factor. Residual correlations were included between the slopes of spatially contiguous ROIs (cf. Carmichael et al., 2013), and the residual variance of regional slope factors whose estimates were negative were constrained to zero to allow the model to converge on in-bounds estimates.

Associations across all cortical factors and all cognitive domains were corrected for multiple comparisons using the False Discovery Rate (FDR; Benjamini & Hochberg, 1995). Comparison of correlation magnitudes was conducted using the Williams (1959) test, implemented in the 'cocor' package (Diedenhofen, 2016) in R. All analyses were conducted in R 3.5.0 ("Joy in Playing"; R Core Team), except for CFA and bivariate growth curve models, which were conducted using MPlus 8.2 (Muthén & Muthén, 2017).

Figure 1. Analysis pipeline for establishing dimensions of brain cortical ageing.

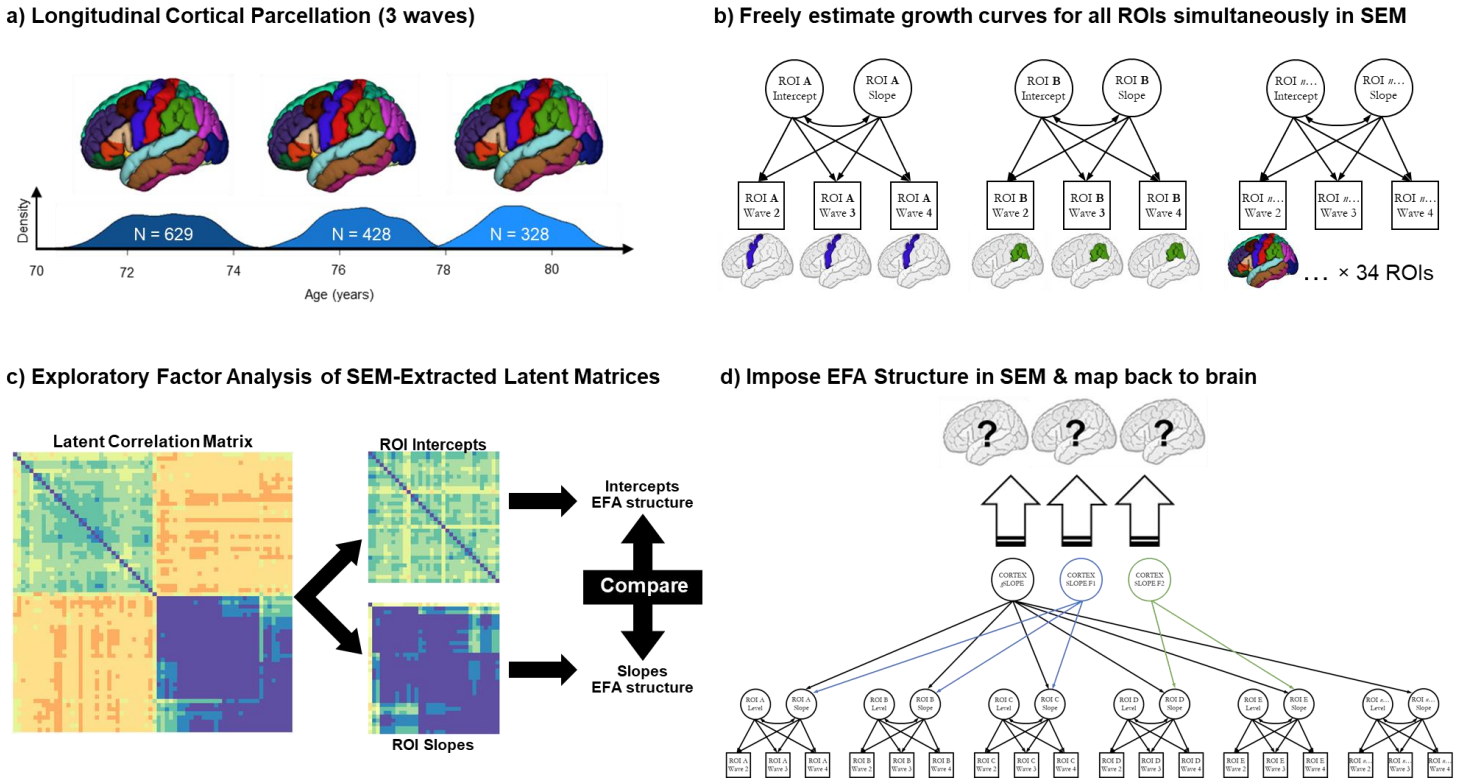

Note. **a)** T1-W brain MRI volumes were parcellated into 34 regions per hemisphere using the FreeSurfer longitudinal pipeline, at 3 waves from c.70-80 years old; **b)** we then simultaneously estimated growth curves (freely-estimated latent intercepts and slopes) for each region of interest (ROI) simultaneously, with a structural equation model (SEM); **c)** we extracted the resultant latent correlation matrix from the SEM in (b), separated these into intercepts and slopes used these matrices to investigate their correlational structure, using a Schmid-Leiman exploratory factor analyses (EFA). We ran formal tests to compare this structure across hemispheres (left v right) and between intercepts and slopes; **d)** we then conducted a confirmatory factor analysis (CFA); here we took the same model as in (b), but now imposed the three-factor structure implied by the EFA in (c), rather than freely estimating the slopes of each ROI. ROI latent intercepts were allowed to covary with all latent factors (not shown). The magnitude of the loadings for each of the factors was then mapped back onto the brain ROIs, indicating the groups of regions where atrophy is correlated, and allowing us to ask how these changes are correlated with genetic and cognitive status (e.g. Figure 4).

Results

Global and Regional Brain Cortical Ageing

Participant characteristics are shown in Table 1. Overall and regional reductions in cortical volume are shown in Figure 2 and Supplementary Table 1. Trajectories for each region are also plotted in Supplementary Figure 3. Overall cortical volume showed a significant decline of 0.87% per annum (3,475mm^3 of baseline volume). However, the rate of annual decline was not consistent across regions. Areas of overall greatest change included frontal and temporal poles (≥ 1.30% reduction per annum) parietal cortex, lateral occipital and lateral aspects of the frontal lobe. In contrast, the insula, cingulate and pre- and post-central areas showed much lower volumetric declines (≤ 0.67% reduction per annum).

Figure 2. Global and regional cortical volumetric change from age 70 to 81 years of age.

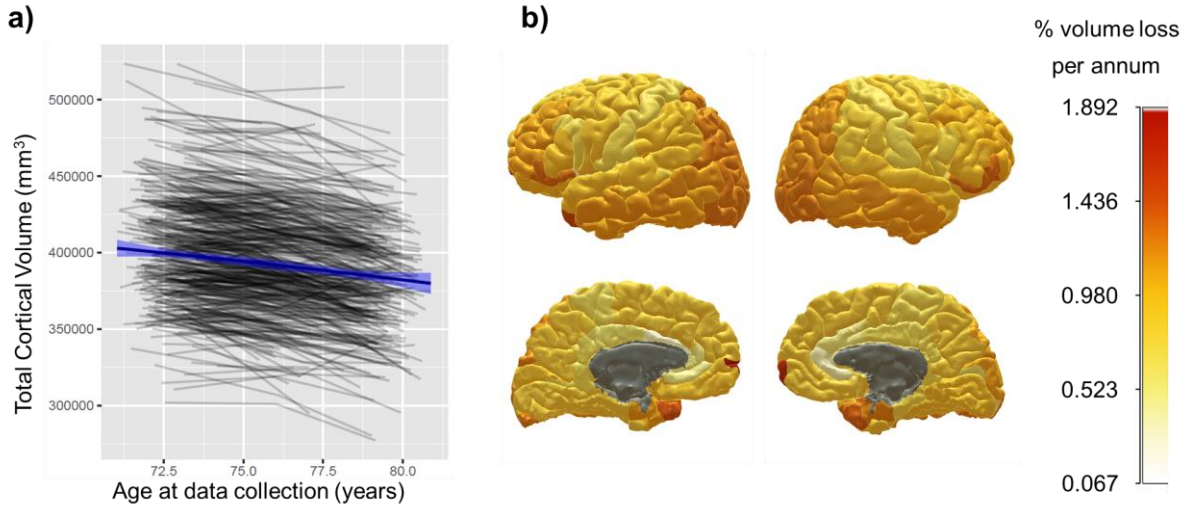

Note. **a)** shows, in grey lines, individual trajectories of global cortical volume; blue line denotes the mean linear trajectory with 95% CIs. **b)** shows the mean % loss per annum, estimated by growth curve models, for each cortical region of interest; warmer colours denote a steeper decline (grey areas indicate non-significant change).

Table 1. Participant characteristics.

	Wave 2		Wave 3		Wave 4	
	M (SD)	**N**	**M(SD)**	**N**	**M(SD)**	**N**
Age (years)	72.49 (0.71)	866	76.24 (0.68)	697	79.32 (0.62)	550
Sex M:F	448:418	866	360:337	697	275:275	550
***APOE* e4 carriers (N:Y)**	575:245	820	459:200	659	365:156	521
Cortical Volume (mm^3)	398508 (396537)	629	393294 (36251)	428	382675 (35046)	328
Matrix Reasoning	13.17 (4.96)	863	13.04 (4.91)	689	12.90 (5.03)	535
Block Design	33.64 (10.08)	864	32.18 (9.95)	691	31.20 (9.63)	535
Spatial Span Forwards	7.63 (1.66)	863	7.57 (1.63)	690	7.40 (1.61)	536
Spatial Span Backwards	7.06 (1.61)	861	7.05 (1.59)	690	6.74 (1.60)	536
Symbol Search	24.61 (6.18)	862	24.60 (6.46)	687	22.73 (6.63)	528
Digit Symbol	56.40 (12.31)	862	53.81 (12.93)	685	51.24 (13.01)	535
Inspection Time	111.22 (11.79)	838	110.14 (12.55)	654	106.96 (13.6)	465
4-Choice Reaction Time	0.65 (0.09)	865	0.68 (0.10)	685	0.71 (0.11)	543
Logical Memory	74.23 (17.89)	864	74.58 (19.20)	688	72.71 (20.39)	542
Verbal Pairs	27.18 (9.46)	843	26.41 (9.56)	663	27.14 (9.55)	497
Digit Span Backwards	7.81 (2.29)	866	7.77 (2.37)	695	7.56 (2.18)	548

Note. Across Wave 2 to 4 (brain imaging data was not collected at Wave 1 of the study).

Factors of Brain Cortical Change

Exploratory Factor Analysis

Across the left hemisphere of the cortical mantle, the rates of the 34 ROIs' cortical changes were highly correlated (average $r = 0.81$, SD = 0.25). These correlations of changes were higher than the correlations between the ROIs' cross-sectional levels (average $r = 0.35$, SD = 0.18). Results of the exploratory Schmid-Leiman analyses are shown in Supplementary Figure 4, and in Supplementary Table 2. Thirty-three of the 34 ROIs loaded on the first unrotated (general) factor, with only 4 of them < 0.5; the mean loading was 0.78. Beyond this general factor, ROI slopes showed two relatively distinct factors that were orthogonal to it; one had larger loadings in mainly fronto-temporal ROIs, and the other had high loadings in predominantly occipito-parietal ROIs. When we conducted the same Schmid-Leiman factor analysis on the right hemisphere data (Supplementary Table 3) and formally compared the factor structure between hemispheres, we found these two be highly similar (Supplementary Table 4; r range 0.61 to 0.78; factor congruence range 0.73 to 0.99). The factor structure for the ROIs' intercepts was consistent between hemispheres. Importantly, however, the slope and intercept factor structure were less similar (r range 0.04 to 0.67; factor congruence range 0.45 to 0.93). Thus, the brain regions' cross-sectional correlational structure showed relatively weak correspondence to the pattern of correlated changes across the cortex.

Given the high level of agreement between left and right hemispheres, we subsequently conducted a Schmid-Leiman analysis for bilateral regional averages (Figure 3 and Supplementary Table 5). A first (unrotated) general factor explained 55% of the variance among cortical volumetric slopes (loadings range 0.50 to 0.82, M = 0.75, SD = 0.09). The other two factors, which are independent of the general factor, accounted for 29% (loadings M = 0.58, SD = 0.13) and 13% (loadings M = 0.49, SD = 0.14) of the slope variance. In contrast, the same analysis of the cortical *intercepts* resulted in a factors that accounted for substantially less variance (General = 27%, Factor 1 = 16%, and Factor 2 = 3%). Again, the factor structure for intercepts and slopes was not similar; their lack of correspondence with the slope factor structure was confirmed through formal tests (Supplementary Table 6), indicating that although factor congruence of the General factor and Factor 1 were good (0.95 and0.88), this was not so for Factor 2 (0.54), nor were the factor loading correlations strong for any factor (r = 0.30, 0.53 and 0.54). Re-running these analyses once participants with a self-reported diagnosis of dementia or MMSE score > 24 (N = 31) or neuroradiologically-identified stroke (N = 119) at any wave had been removed did not substantially alter the patterns (Supplementary Tables 7 and 8, and Supplementary Figures 5 and 6).

Figure 3. Correlation matrices and exploratory factor loadings for ROI intercepts and slopes, estimated using left-right average values for ROIs.

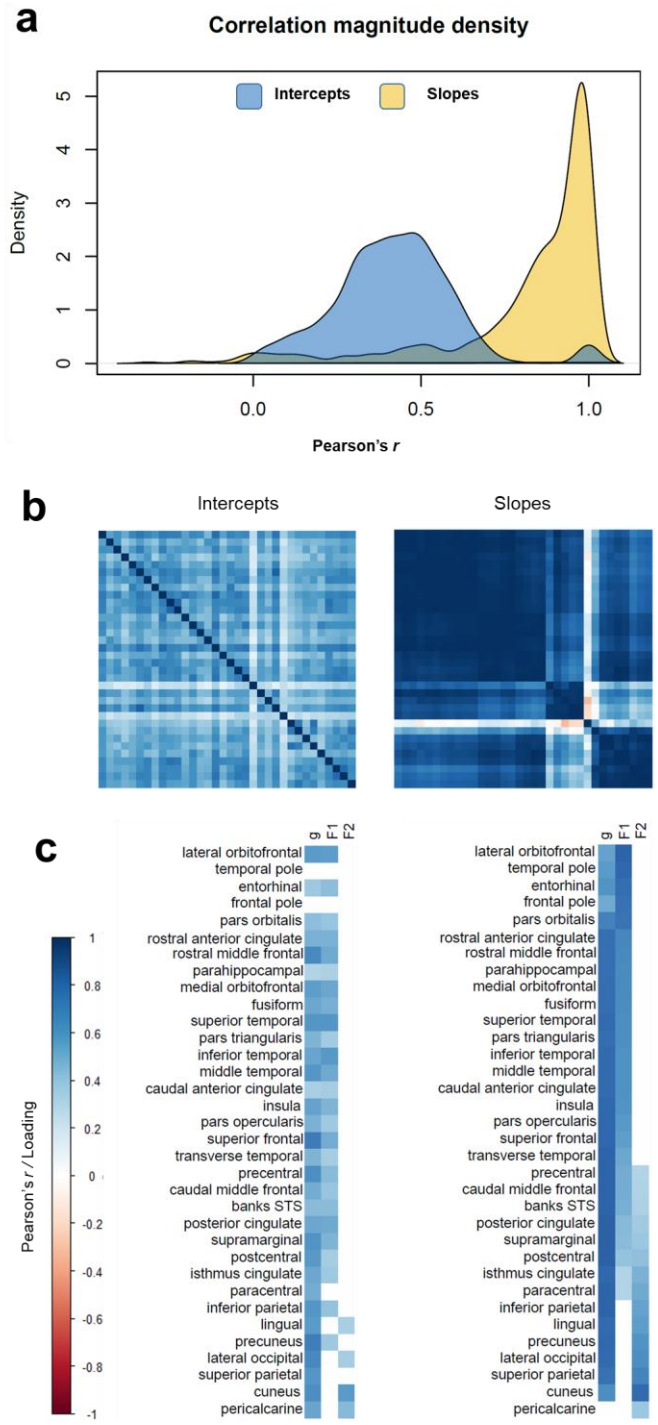

Note. Exploratory factor analyses. **(a)** density plots of the correlation magnitudes among freely-estimated intercepts and slopes; **(b)** heatmaps of the correlations among freely-estimated latent intercepts (left) and slopes (right), intercept axes are fixed according to the hierarchically-clustered slope matrix; **(c)** loadings of each ROI's intercept and slope on a general factor of cortical change ("*g*") and on two additional factors identified from an exploratory Schmid-Leiman factor analysis, conducted on the same latent correlation matrices as shown in (b). Loadings reported in Supplementary Table 5. Factor F1 pertains to fronto-temporal, and F2 to occipito-parietal regions.

Confirmatory Factor Analysis – mapping back to the brain

We then undertook a confirmatory factor analysis (CFA) SEM. Here, we used the loading structure for the ROI changes that we had discovered from our EFA, and formally modelled the structure (a bifactor model, with one global factor, and two subsequent factors) in SEM. We wanted to ascertain the goodness of fit, map the standardised loadings back to the brain, and then ask how these observed factors of brain change were associated with *APOE* status and cognitive declines. Factor loadings from the CFA are plotted onto the cortical surface in Figure 4 (and are also provided in Supplementary Table 9). The CFA showed good fit to the data (Supplementary Table 10), and the brain cortical ROIs' slope loadings on the three slope factors were highly commensurate with the exploratory findings (Supplementary Figure 7). The global factor showed general loadings across the cortex, whereas Factor 1 pertained clearly to frontal and temporal regions and Factor 2 related to occipital and parietal cortex; we shall henceforth refer to these as fronto-temporal and posterior-parietal factors, respectively. These factors explained a total of 86% of the total variance in regional slopes (general factor = 63%, fronto-temporal factor = 16%, and occipito-parietal factor = 7%). It is noteworthy that, although we refer to this largest factor as 'general' (as it is indicated by all but one region - pericalcarine), the actual magnitude of the CFA-estimated loadings ranged from 0.348 to 1.00, though most were large (M = 0.79, SD = 0.18; Supplementary Table 9). Loadings were strongest (>0.80) in the insula, dorsolateral and medial prefrontal, cingulate, lateral temporal and inferior parietal areas. In contrast, ventrolateral frontal, medial temporal, superior parietal and cuneal cortex showed relatively lower loadings (range 0.348 to 0.670). Fronto-temporal factor and occipito-parietal factor —which are independent of (orthogonal to) the general factor—were negatively correlated (r = -0.254, $p < 0.001$), indicating that participants exhibiting greater fronto-temporal decline tended to show less occipito-parietal decline, for any given level of global cortical volume change. Females and males did not differ in their trajectories of any aspect of cortical change (general = 0.020, p = 0.726, fronto-temporal = 0.020, p = 0.735, occipito-parietal = -0.005, p = 0.911).

Figure 4. Cortical patterning of factors of cortical ageing

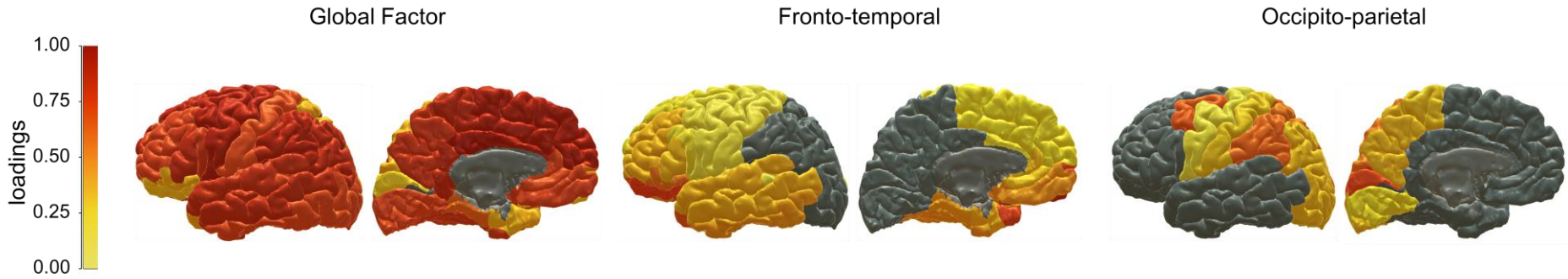

Note. Warmer colours denote stronger standardised factor loadings of each ROI volume on each of the factors of cortical change estimated in the confirmatory factor analysis (see Supplementary Table 9). Grey colour denotes no loading. All ROIs except the pericalcarine cortex loaded onto the general factor, with subsequent loadings on Factors 1 (fronto-temporal) or Factor 2 (occipito-parietal) indicating that these ROIs exhibited common ageing trajectories in addition to the global pattern of overall cortical decline.

Figure 5. Modelling the coupled changes between cortical factors and cognitive domains.

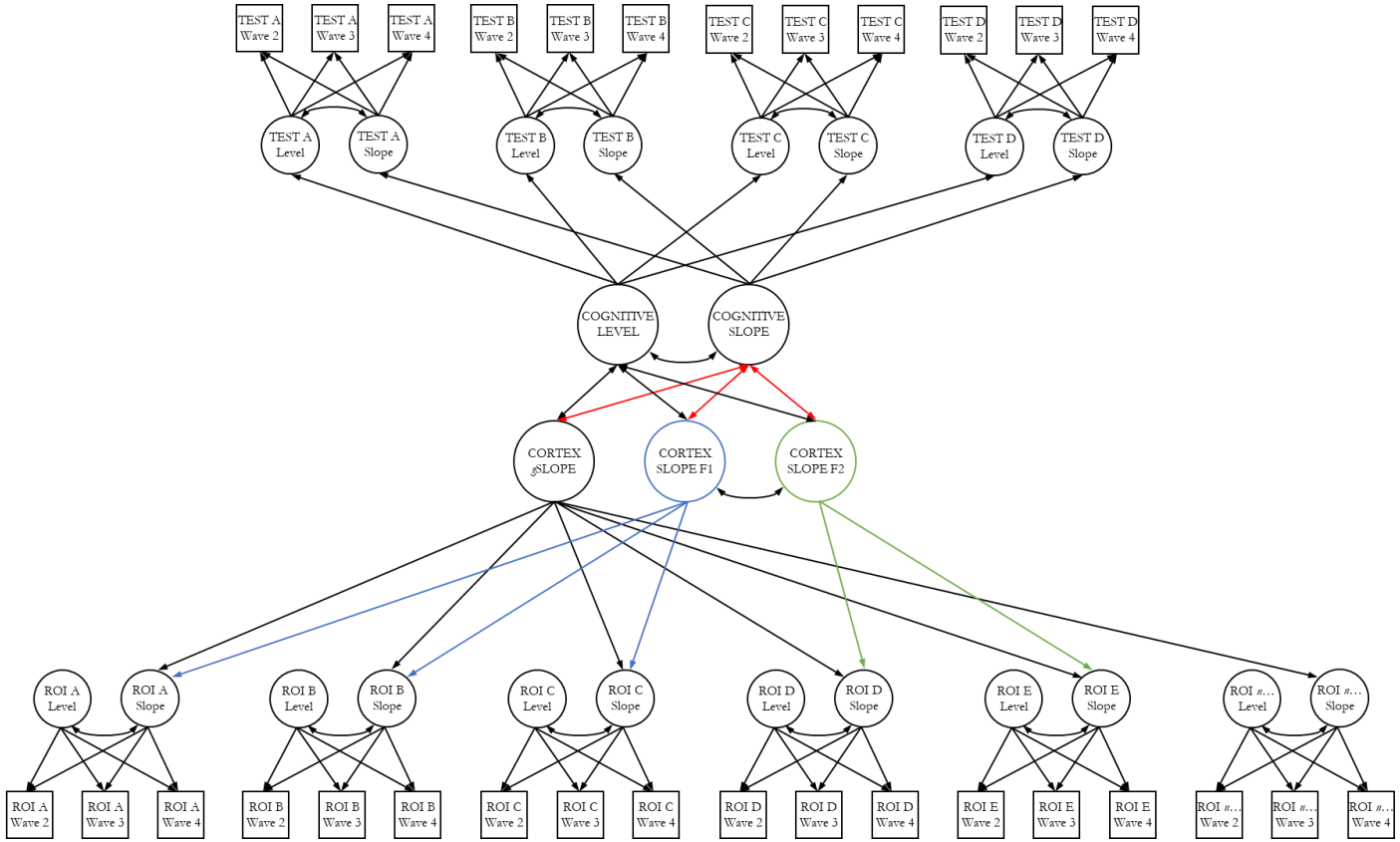

Note. An example of a multivariate latent growth curve model assessing associations between cortical and cognitive changes. The top half of the model illustrates how the intercept and slope of a given cognitive domain is indicated by the individual intercept and slope of multiple individual cognitive tests, tested on 3 occasions. The bottom half of the model illustrates how the 3 factors of cortical change are differentially indicated by the individual slopes of each of 34 cortical regions of interest (ROI). Residual correlations among manifest variables not shown. ROI intercept factors were freely estimated and allowed to correlate with all latent factors (not shown to reduce figure complexity). Red paths denote associations of interest, between cognitive and cortical changes. The two 'secondary' factors of cortical volume (F1 and f2) are orthogonal to the general slope of cortical volume, and negatively correlated with each other (r = -0.254, $p < 0.001$).

Are patterns of cortical ageing related to *APOE* e4 status and cognitive decline?

An example of the multivariate SEM correlating cortical and cognitive ageing is shown in Figure 5. Measurement models of the cognitive domains, and the multivariate models correlating MRI with *APOE* and cognitive measures all showed good fit to the data (Supplementary Table 11). *APOE* e4 carriers exhibited steeper atrophy for the general factor (r = -0.100, p = 0.038), but the statistical significance of this association did not survive FDR correction (Table 2). *APOE* e4 carriers did not show significantly steeper cortical atrophy on either fronto-temporal or occipito-parietal factors (r = -0.044, p = 0.414; r = 0.012, p = 0.774, respectively).

Associations between the changes in cognitive domains and brain cortical factors are shown in Table 2. Trajectories of cognitive change in this sample have already been characterised and reported previously (Ritchie et al., 2016). Greater cortical volumetric decline at the global level was significantly associated with declines in general cognitive ability (g) (r = 0.430, p < 0.001), processing speed (r = 0.383, p < 0.001), and memory ability (r = 0.372, p < 0.001), but not with visuospatial ability (r = 0.143, p = 0.151). No other correlations among cognitive changes and either of the secondary factors of cortical change were FDR-significant (all rs ≤ |0.186|).

Table 2. Associations between factors of cortical change and *APOE* status, and changes in cognitive domains.

	Global Factor	**Fronto-temporal Factor**	**Occipito-parietal Factor**
***APOE* e4 carrier**	-0.100 (0.038)	-0.044 (0.414)	0.012 (0.774)
g	**0.430 (<0.001)**	-0.005 (0.942)	-0.078 (0.174)
Visuospatial	0.140 (0.162)	-0.165 (0.105)	-0.185 (0.031)
Processing Speed	**0.369 (<0.001)**	-0.010 (0.893)	-0.066 (0.256)
Memory	**0.363 (<0.001)**	0.066 (0.352)	-0.026 (0.644)

Note. Standardised estimates (p-values) are reported for associations between the three factors of cortical volumetric change (global, fronto-temporal and posterior-parietal), *APOE* status (where 1 = at least 1 × e4 allele), and the three cognitive domains (visuospatial, processing speed and memory). Bold typeface denotes FDR-q < 0.05.

Discussion

In this cohort of community-dwelling older adults, assessed three times over the course of their 8th decade, we identified three axes of cortical change, along which general and anatomically-localised atrophy occurs. That is, we identified three dimensions of cortical atrophy which described clusters of areas exhibiting correlated rates of ageing. Together, these three patterns explained 83% of the individual differences in cortical ageing across 34 bilateral ROIs. Changes across the cortex were, in general, strongly correlated, and a general factor accounted for 63% of volumetric changes across the 34 ROIs. This general factor was associated with declines in a measure of general cognitive function ('g'), which was more strongly driven by processing speed and memory than by visuospatial declines. Two additional, mildly-negatively-correlated factors existed on an anterior-posterior axis, and together explained an additional 20% of the variation in cortical ageing. Thus, for any given level of global cortical ageing, individuals tend additionally to experience either more fronto-temporal or more occipito-parietal cortical ageing. However, change across either of these additional dimensions of cortical atrophy were not significantly related to any latent measures of cognitive decline, beyond the principal axis of cortical atrophy.

Just as differential psychology has determined that a single psychological factor may largely underlie age-related declines across multiple cognitive tests (Tucker-Drob et al., 2019), so the current findings indicate that a large proportion of cortical atrophy occurs across a single dimension – and furthermore, that general cortical and general cognitive ageing are significantly coupled. By identifying that changes in both cognitive abilities and cortical volumes appear to occur along general – and correlated – statistical dimensions, these findings and similar approaches represent an important step in guiding ongoing research into the neuroanatomical correlates and potential underlying mechanisms of cognitive ageing. With respect to the interpretation of the general factor of cortical change, we note that fronto-temporal changes are more representative of overall cortical change: these lobes comprise a larger proportion of overall cortex, and our general factor was indicated by a far greater proportion of frontal and temporal parcels (N = 22) than parietal and occipital parcels (N = 12), and showed some subtle variation in loading magnitudes (though most were uniformly large). As such, we interpret the general cortical factor - and its correlations with cognitive ageing - as pertaining more strongly to fronto-temporal than occipito-parietal cortex.

Strikingly, the patterns of structural covariance in cortical *changes* departed substantially from those observed in concurrent patterns of structural covariance among *levels* at baseline. Correlations among baseline ROI volumes were moderate (average $r = 0.350$, SD = 0.178) in magnitude, yet markedly weaker than correlations among rates of longitudinal atrophy (average $r = 0.805$, SD = 0.252). There was only a subtle resemblance between the factors structure for level and change; a result that underscores previous claims for the theoretical and empirical strengths of using longitudinal data to inform accounts of ageing (Raz & Lindenberger, 2011; Salthouse, 2011). Only longitudinal data can be used to directly estimate

the dimensionality of change over time, and to distinguish lifelong patterns of structural covariance from patterns that are specific to ageing.

We showed that the factor structure of cortical decline did not change when we removed those who had some indication of dementia, or stroke, suggesting that these patterns are also present in ostensibly 'healthy' ageing. The fronto-temporal pattern is partly consistent with frontal ageing accounts of cognitive decline (MacPherson et al., 2002; Buckner et al., 2004), and with the partial overlap between fronto-temporal ageing in healthy and Alzheimer's-type patterns (e.g. Habes et al., 2016). It is also notable that these three factors of change are similar to three of the five aspects of cortical change identified using a similar factor analytic method, in participants with MCI (Carmichael et al., 2013). They found that individuals with greater frontal and temporal change, but not a more posterior pattern, were significantly more likely to convert to a clinical diagnosis of Alzheimer's disease. Moreover, these anterior and posterior patterns are similar to neurobiological patterns of dementia subtypes such as fronto-temporal and posterior cortical degeneration. Fronto-temporal lobar degeneration is a well-known pattern in pathological ageing, representing one of the main causes of dementia (accounting to up to 10% of all dementias; Seltman and Matthews, 2012). In contrast, posterior cortical atrophy (PCA) is characterised by selective decline in functions mainly reliant on parietal and occipital brain regions (Crutch et al., 2012; Firth et al., 2019). It is estimated to account for around 8% of Alzheimer's disease cases (Snowden et al., 2007), though its prevalence is currently unknown, and it is relatively under-researched (Crutch et al., 2012). These apparent similarities should be interpreted with additional caution though, given that none of the cortical changes were significantly steeper in carriers of the *APOE* e4 allele, which is a well-known risk factor for late-life dementia (Liu et al., 2013).

The study has limitations. Whereas it is tempting to draw parallels between the patterns of cortical atrophy identified here and those observed in clinical subtypes, volumetric atrophic effects likely reflect numerous ongoing processes. On the other hand, we were unable to rule out the influence of nascent clinical neurodegeneration on the patterns of cortical atrophy discovered here, which we based on self-reported dementia and MMSE scores. It is possible that these additional profiles (anterior and posterior) reflect nascent and separable pathological neurodegenerative processes. Whereas we consider it unlikely that our results are predominantly driven by such effects (given the general prevalence of these cases in the population; Snowden et al., 2007; Seltman and Matthews, 2012), neurostructural hallmarks may be detectable prior to the onset of cognitive impairments (Jack Jr et al., 2013). It may therefore be of interest to test whether these additional patterns of cortical change, which we identified in the eighth decade of life, predict future cognitive trajectories as longitudinal testing continues into older ages. There are also many other aspects of brain structure and function that were not measured which may shed further light on any potential similarities and differences with pathological ageing. Moreover, the present results indicate that these additional patterns are relatively subtle among relatively healthy and range restricted (Johnson et al., 2016) group of older adults. As such, it is possible that these are underestimates of the true extent to which these patterns are present at the population level. Finally, in the move from exploratory to confirmatory factor analyses, it would have been

ideal to have a second narrow-age-range sample with longitudinal imaging across this period of life in which to replicate the observed patterns of cortical atrophy. In the absence of an appropriate replication sample, we conducted a pseudo-replication of the pattern between hemispheres, though we acknowledge that this is suboptimal.

In summary, our analyses have revealed that i) cortical ageing occurs partly as a coordinated mantle-wide process, and beyond that, as either greater fronto-temporal or greater occipito-parietal atrophy; ii) this same pattern is not readily apparent from cross-sectional data; iii) the major, single/general, axis of cortical atrophy (indicated by a greater number of fronto-temporal regions) is related to general cognitive decline, and processing speed and memory cognitive ability domains.

Author Contributions

SRC, IJD and ETD designed the analysis. SRC conducted the analysis and drafted the work. MEB, JMW and IJD conceived the study design, SRC, MH, MVH, JC, AT and JMW collected or analysed the brain MRI and/or cognitive data. All authors substantively revised the work and have approved the submitted version.

Data and Code Availability

Materials, code, and associated protocols will be made available upon reasonable request to the corresponding author. The data analysed in this study is not publicly available as it contains data that could compromise participant consent and confidentiality, but can be requested via a data access request to the Lothian Birth Cohorts research group.

Acknowledgements

We thank the Lothian Birth Cohort 1936 members who took part in this study, and Lothian Birth Cohort 1936 research team members who collected, entered and checked data used in this manuscript. The LBC1936 and this research are supported by Age UK (Disconnected Mind project) and by the UK Medical Research Council [MRC; G0701120, G1001245, MR/M013111/1]. SRC, SJR, MEB, IJD and EMT-D were also supported by a National Institutes of Health (NIH) research grant R01AG054628. MH, AMM, HCW, JMW, IJD are also supported by a Wellcome Trust Strategic Award (Ref 104036/Z/14/Z). MCVH is funded by the Row Fogo Charitable Trust (grant No. BROD.FID3668413). EMT-D is a member of the Population Research Center at the University of Texas at Austin, which is supported by NIH center grant P2CHD042849. TCR is a member of the Alzheimer Scotland Dementia Research Centre supported by Alzheimer Scotland.

References

Bárrios H, Narciso S, Guerreiro M, Maroco J, Logsdon R et al. Quality of life in patients with mild cognitive impairment. Ageing and Mental Health, 2013;17:287-292.

Benjamini Y, Hochberg Y. Controlling the false discovery rate: a practical and powerful approach to multiple testing. Journal of the Royal Statistical Society, 1995;57:289-300.

Buckner RL. Memory and executive function in aging and AD: multiple factors that cause decline and reserve factors that compensate. Neuron 2004;44:195-208.

Burt C. The factorial study of temperamental traits. British Journal of Statistical Psychology, 1948;1:178-203.

Carmichael I, McLaren DG, Tommet D, Mungas D, Jones RN et al. Coevolution of brain structures in amnestic mild cognitive impairment. Neuroimage, 2013; 66:449-456.

Corley J, Cox SR, Deary IJ. Healthy cognitive ageing in the Lothian Birth Cohort studies: marginal gains not magic bullet. Psychological Medicine, 2018;48:187-207.

Cox SR, Ritchie SJ, Tucker-Drob EM, Liewald DC, Hagenaars SP et al. Ageing and brain white matter structure in 3,513 UK Biobank participants. Nat Commun 2016; 7:13629.

Crutch SJ, Lehmann M, Schott JM, Rabinovici GD, Rossor MN, Fox NC. Posterior cortical atrophy. Lancet Neurology, 2012; 11:170-178.

Deary IJ, Penke L, Johnson W. The neuroscience of human intelligence differences. Nature Reviews Neuroscience, 2010; 11:201-211.

Deary IJ, Gow AJ, Pattie A, Starr JM. Cohort profile: the Lothian Birth Cohorts of 1921 and 1936. International Journal of Epidemiology, 2012;41:1576-1584.

Diedenhofen B. 2016. Package 'cocor'. https://cran.r-project.org/web/packages/cocor/cocor.pdf

Doan NT, Engvig A, Zaske K, Persson K, Lund MJ et al. Distinguishing early and late brain aging from the Alzheimer's disease spectrum: consistent morphological patterns across independent samples. Neuroimage, 2017;158:282-295.

Douaud G, Groves AR, Tamnes CK, Westlye LT et al. A common brain network links development, aging and vulnerability to disease. Proceedings of the National Academy of Sciences, 2014;111:17648-17653.

Doucet GE, Moser DA, Rodrigue A, Bassett DS, Glahn DC et al. Person-based brain morphometric similarity is heritable and correlates with biological features. Cerebral Cortex, 2019; 29:852-862.

Fineberg NA, Haddad PM, Capenter L, Gannon B, Sharpe R et al. The size, burden and cost of disorders of the brain in the UK. Journal of Psychopharmacology, 2013;27:761-770.

Firth NC, Primativo S, Marinescu R-V, Shakespeare TJ, Suarez-Gonzalez A, et al. Longitudinal neuroanatomical and cognitive progression of posterior cortical atrophy. Brain, 2019;142:2082-2095.

Fjell AM, Walhovd KB. Structural brain changes in aging: courses, causes and cognitive consequences. Rev Neuosci 2010;21:187-221.

Fjell AM, Walhovd KB. Neuroimaging results impose new views on Alzheimer's disease-the role of amyloid revised. Molecular Neurobiology. 2012;45:153–17

Fjell AM, McEvoy L, Holland D, Dale AM, Walhovd KB. What is normal in normal aging? Effects of aging, amyloid and Alzheimer's disease on the cerebral cortex and the hippocampus. Prog Neurobiol 2014;117:20-40.

Folstein MF, Folstein SE, McHugh PR. "Mini-mental status". A practical method for grading the cognitive state of patients for the clinician. Journal of Psychiatric Research, 1975;12:189–198.

Habes M, Janowitz D, Erus G, Toledo JB, Resnick SM et al. Advanced brain aging: relationship with epidemiologic and genetic risk factors, and overlap with Alzheimer disease atrophy patterns. Translational Psychiatry 2016;6:e775.

Hafkemeijer A, Altmann-Schneider I, de Craen AJM, Slagboom PE, van der Grond et al. Associations between age and gray matter volume in anatomical brain networks in middle-aged to older adults. Aging Cell, 2014;13:1068-1074.

Jack Jr, CR, Knopman DS, Jagust WJ, Petersen RC, Weiner MW et al. Tracking pathophysiological processes in Alzheimer's disease: an updated hypothetical model of dynamic biomarkers. Lancet Neurol 2013;12:207-216.

Johnson W, Brett CE, Calvin C, Deary IJ. Childhood characteristics and participation in Scottish Mental Survey 1947 6-day sample follow-ups: Implications for participation in aging studies. Intelligence, 2016;54:70-79.

Kong X-Z, Mathias SR, Guadalupe T, ENIGMA Laterality Working Group, Glahn DC et al. Mapping cortical brain asymmetry in 17,141 heathy individuals worldwide via the ENIGMA Consortium. PNAS, 2018;115:E5154-E5163.

Liu CC, Liu CC, Kanekiyo T, Xu H, Bu G. Apolipoprotein E and Alzheimer's disease: risk, mechanisms and therapy. Nature Reviews Neurology, 2013;9:106-118.

Molenaar PCM. A manifesto on Psychology as idiographic science: bringing the person back into scientific psychology, this time forever. Measurement, 2004;2:911-913.

Muthén LK, Muthén BO. 1998-2017, Mplus User's Guide. Eighth Edition, Los Angeles, CA: Muthén & Muthén.

Prince M, Knapp M, Guerchet M, McCrone P, Prina M et al. Dementia UK: Update. Alzheimer's Society 2014 ISBN: 978-1-906647-31-5

Raz N, Lindenberger U. Only Time will Tell: Cross-sectional Studies Offer no Solution to the Age-Brain-Cognition Triangle—Comment on Salthouse (2011). Psychological Bulletin, 2011;137:790-795.

Revelle, W. 2019. Package 'psych'. https://cran.r-project.org/web/packages/psych/psych.pdf

Ritchie SJ, Tucker-Drob EM, Starr JM, Deary IJ. Do cognitive and physical functions age in concert from age 70 to 76? Evidence from the Lothian Birth Cohort 1936. Spanish Journal of Psychology, 2016; 19:1-12.

Rosseel, Y. lavaan: An R package for structural equation modeling. Journal of Statistical Software, 2012;48:1-36.

Salthouse TA. Neuroanatomical substrates of age-related cognitive decline. Psychological Bulletin, 2011;137:753-784.

Schmid J, Leiman JM. The development of hierarchical factor solutions. Psychometrika, 1957;22:53-61.

Seltman, R. E., and Matthews, B. R. Frontotemporal lobar degeneration: epidemiology, pathology, diagnosis and management. CNS Drugs 2012; 26: 841–870.

Smith SM, Elliott LT, Alfaro-Almagro F, McCarthy P, Nichols TE et al. Brain aging comprises multiple modes of structural and functional change with distinct genetic and biophysical associations. bioRvix, 2019; https://www.biorxiv.org/content/10.1101/802686v1.full.

Snowden JS, Stopford CL, Julien CL…. Cognitive phenotypes in Alzheimer's disease and genetic risk. Cortex, 2007; 43:835-845.

Takao H, Abe O, Yamasue H, Aoki S, Kasai K et al. Aging effects of cerebral asymmetry: a voxel-based morphometry and diffusion tensor imaging study. Magnetic Resonance Imaging, 2010;28:65-69.

Taylor AM, Pattie A, Deary IJ. Cohort Profile Update: The Lothian Birth Cohorts of 1921 and 1936. International Journal of Epidemiology, 2018;47:1042-1042r.

Tucker-Drob EM, Brandmaier AM, Lindenberger U. Coupled cognitive changes in adulthood: a meta-analysis. Psychological Bulletin, 2019; 143:273-301.

Tucker-Drob EM, Briley DA, Starr JM, Deary IJ. Structure and correlates of cognitive aging in a narrow age cohort. Psychology and Aging, 2014; 29:236-249.

Wardlaw JM, Bastin ME, Valdés Hernández MC, Muñoz Maniega S, Royle NA et al. Brain aging, cognition in youth and old age and vascular disease in the Lothian Birth Cohort 1936: rationale, design and methodology of the imaging protocol. International Journal of Stroke, 2011; 6:547-559.

Wardlaw JM, Valdés Hernández MC, Muñoz Maniega S. What are white matter hyperintensities made of? J Am Heart Assoc 2015;4:e001140.

Wenham PR, Price WM, Blandell G. Apolipoprotein E genotypic by one-stage PCR. Lancet, 1991;337:1158-1159.

Williams EJ . The comparison of regression variables. Journal of the Royal Statistical Society, Series B, 1959;21:396-399. Retrieved from http://www.jstor.org/stable/2983809

Wimo A, Jönsson L, Bond J, Prince M, Winblad B et al. The worldwide economic impact of dementia 2010. Alzheimer's and Dementia, 2013;9:1-11.e3.

Supplementary Material

Supplementary Table 1. Estimates of regional cortical change.

	Hemi	*β*	SE	*p*	% loss p.a.
GLOBAL					
Volume (cm^3)		-3.475	0.130	<0.001	0.872
REGIONAL VOLUME					
Banks STS	L	-1.580	0.123	0.000	-0.761
	R	-1.649	0.105	0.000	-0.840
Caudal ACC	L	-0.306	0.109	0.005	-0.211
	R	-0.705	0.123	0.000	-0.410
Caudal Middle Frontal	L	-4.505	0.294	0.000	-0.844
	R	-3.889	0.272	0.000	-0.772
Cuneus	L	-2.260	0.137	0.000	-0.864
	R	-2.828	0.135	0.000	-1.026
Entorhinal	L	-1.947	0.202	0.000	-1.059
	R	-1.982	0.163	0.000	-1.147
Frontal Pole	L	-1.596	0.073	0.000	-1.892
	R	-1.900	0.092	0.000	-1.720
Fusiform	L	-7.041	0.547	0.000	-0.787
	R	-7.071	0.493	0.000	-0.821
Inferior Parietal	L	-13.632	0.543	0.000	-1.215
	R	-15.137	0.605	0.000	-1.141
Inferior Temporal	L	-10.440	0.503	0.000	-1.048
	R	-10.652	0.477	0.000	-1.105
Insula	L	-1.717	0.314	0.000	-0.265
	R	-1.946	0.376	0.000	-0.297
Isthmus Cingulate	L	-1.506	0.145	0.000	-0.604
	R	-1.419	0.131	0.000	-0.620
Lateral Occipital	L	-13.191	0.453	0.000	-1.224
	R	-13.365	0.435	0.000	-1.228
Lateral Orbitofrontal	L	-6.154	0.370	0.000	-0.908
	R	-5.546	0.365	0.000	-0.837
Lingual	L	-4.641	0.287	0.000	-0.789
	R	-5.112	0.288	0.000	-0.849
Medial Orbitofrontal	L	-4.520	0.335	0.000	-0.877
	R	-3.724	0.327	0.000	-0.761
Middle Temporal	L	-10.108	0.442	0.000	-1.107
	R	-11.366	0.496	0.000	-1.093
Paracentral	L	-1.770	0.158	0.000	-0.586
	R	-1.995	0.158	0.000	-0.596
Parahippocampal	L	-1.418	0.171	0.000	-0.770
	R	-1.119	0.148	0.000	-0.660
IFG Pars Opercularis	L	-2.633	0.173	0.000	-0.660
	R	-2.501	0.156	0.000	-0.748
IFG Pars Orbitalis	L	-2.402	0.127	0.000	-1.246
	R	-3.007	0.133	0.000	-1.301
IFG Pars Triangularis	L	-2.654	0.151	0.000	-0.897
	R	-3.153	0.162	0.000	-0.901
Pericalcarine	L	-1.027	0.082	0.000	-0.594
	R	-1.027	0.098	0.000	-0.531
Postcentral	L	-5.640	0.389	0.000	-0.659
	R	-5.378	0.398	0.000	-0.667
Posterior Cingulate	L	-1.390	0.184	0.000	-0.502
	R	-1.610	0.169	0.000	-0.587
Precentral	L	-9.581	0.572	0.000	-0.846
	R	-9.874	0.557	0.000	-0.875
Precuneus	L	-6.721	0.408	0.000	-0.807
	R	-6.621	0.391	0.000	-0.779
Rostral ACC	L	-0.986	0.140	0.000	-0.430

	R	-0.447	0.132	0.001	-0.242
Rostral Middle Frontal	L	-13.632	0.631	0.000	-1.066
	R	-13.553	0.616	0.000	-1.018
Superior Frontal	L	-15.113	0.810	0.000	-0.790
	R	-14.234	0.769	0.000	-0.774
Superior Parietal	L	-13.907	0.662	0.000	-1.177
	R	-12.900	0.638	0.000	-1.095
Superior Temporal	L	-8.502	0.459	0.000	-0.872
	R	-8.426	0.461	0.000	-0.880
Supramarginal	L	-8.396	0.419	0.000	-0.887
	R	-7.141	0.391	0.000	-0.792
Temporal Pole	L	-3.913	0.266	0.000	-1.444
	R	-3.323	0.245	0.000	-1.337
Transverse Temporal	L	-1.032	0.055	0.000	-1.043
	R	-0.808	0.045	0.000	-1.050

Supplementary Table 2. Loadings of an exploratory analysis using Schmid-Leiman transform of left hemisphere ROI growth curves.

Region of Interest	*g*	F1	F2
Lateralorbitofrontal	0.60	0.77	
Temporalpole	0.65	0.75	
Entorhinal	0.68	0.70	
Parsorbitalis	0.72	0.69	
Frontalpole	0.68	0.67	
Parstriangularis	0.78	0.59	
Insula	0.77	0.58	
Rostralmiddlefrontal	0.81	0.56	
Parahippocampal	0.80	0.53	
Rostralanteriorcingulate	0.83	0.51	
Superiortemporal	0.83	0.50	
Middletemporal	0.83	0.49	
Fusiform	0.83	0.49	
Parsopercularis	0.83	0.48	
Inferiortemporal	0.83	0.47	
Medialorbitofrontal	0.84	0.45	0.31
Superiorfrontal	0.84	0.41	0.35
Transversetemporal	0.84	0.38	0.38
Caudalanteriorcingulate	0.83	0.38	0.38
Caudalmiddlefrontal	0.84	0.36	0.41
Precentral	0.84	0.36	0.40
Cuneus	0.58		0.78
Superiorparietal	0.69		0.71
Lateraloccipital	0.74		0.68
Precuneus	0.75		0.66
Lingual	0.75		0.64
Inferiorparietal	0.77		0.64
Paracentral	0.77		0.62
Isthmuscingulate	0.79		0.59
Posteriorcingulate	0.82		0.53
Postcentral	0.82		0.52
Supramarginal	0.83		0.48
Banksttsts	0.83		0.47
Pericalcarine			

Note. Loadings for left hemisphere ROIs; values <0.3 not shown (pericalcarine does not load on any of the three factors). Eigenvalues are: *g* = 20.1, F1 = 6.60, F2 = 6.00. General factor loadings of F1 and F2 on *g* were constrained to equality, F1 ~ F2 *r* = 0.544. The S-L transform takes a factor or PC solution, transforms it to an oblique solution, factors the oblique solution to find a higher order (*g*) factor, and then residualizes *g* out of the group factors.

Supplementary Table 3. Loadings of an exploratory analysis using Schmid-Leiman transform of right hemisphere ROI growth curves.

Region of Interest	*g*	F1	F2
Lateralorbitofrontal	0.47	0.84	
Temporalpole	0.37	0.85	
Entorhinal	0.48	0.84	
Parsorbitalis	0.60	0.80	
Frontalpole	0.34	0.65	
Parstriangularis	0.65	0.75	
Insula	0.55	0.76	
Rostralmiddlefrontal	0.63	0.76	
Parahippocampal	0.56	0.77	
Rostralanteriorcingulate	0.58	0.81	
Superiortemporal	0.63	0.78	
Middletemporal	0.61	0.79	
Fusiform	0.64	0.77	
Parsopercularis	0.66	0.74	
Inferiortemporal	0.63	0.78	
Medialorbitofrontal	0.60	0.80	
Superiorfrontal	0.68	0.72	
Transversetemporal	0.69	0.69	
Caudalanteriorcingulate	0.62	0.77	
Caudalmiddlefrontal	0.70	0.68	
Precentral	0.70	0.68	
Cuneus	0.67	0.71	
Superiorparietal	0.71	0.65	
Lateraloccipital	0.73	0.59	0.34
Precuneus	0.70	0.67	
Lingual	0.64	0.54	
Inferiorparietal	0.73	0.59	0.34
Paracentral	0.74	0.56	0.38
Isthmuscingulate	0.71	0.53	0.38
Posteriorcingulate	0.74	0.46	0.49
Postcentral	0.74	0.43	0.51
Supramarginal	0.73	0.33	0.60
Banksttsts	0.71		0.68
Pericalcarine			0.59

Note. Loadings for right hemisphere ROIs; values <0.3 not shown (pericalcarine does not load on any of the three factors). Eigenvalues are: g = 20.1, F1 = 6.60, F2 = 6.00. General factor loadings of F1 and F2 on g were constrained to equality, F1 ~ F2 r = 0.383. The S-L transform takes a factor or PC solution, transforms it to an oblique solution, factors the oblique solution to find a higher order (g) factor, and then residualizes g out of the the group factors.

Supplementary Table 4. Comparisons of factor structure between left and right hemispheres as identified by the exploratory Schmid-Leiman analysis of ROI slopes and intercepts.

		LOADINGS	
Correspondence	**General Factor**	**Factor 1**	**Factor 2**
SLOPES			
Left vs Right Hemisphere			
Pearson's	0.78	0.70	0.61
Factor Congruence	0.99	0.87	0.73
INTERCEPTS			
Left vs Right Hemisphere			
Pearson's *r*	0.97	0.76	0.90
Factor Congruence	1.00	0.92	0.91
SLOPES versus INTERCEPTS			
Left vs Left & Right vs Right Hemisphere			
Pearson's *r*	L (0.05) R (0.04)	L (0.29) R (0.51)	L (0.32) R (0.67)
Factor Congruence	L (0.91) R (0.93)	L (0.74) R (0.86)	L (0.45) R (0.70)

Note. Standardised loadings are reported; L = left hemisphere; R = right hemisphere.

Supplementary Table 5. Loadings of an exploratory factor analysis using Schmid-Leiman transform of left-right averaged ROI growth curves.

Region of Interest	*g*	F1	F2
Lateralorbitofrontal	0.53	0.80	
Temporalpole	0.56	0.79	
Entorhinal	0.60	0.77	
Frontalpole	0.50	0.75	
Parsorbitalis	0.68	0.73	
Rostralanteriorcingulate	0.75	0.65	
Rostralmiddlefrontal	0.75	0.64	
Parahippocampal	0.75	0.64	
Medialorbitofrontal	0.76	0.64	
Fusiform	0.76	0.63	
Superiortemporal	0.77	0.61	
Parstriangularis	0.77	0.61	
Inferiortemporal	0.78	0.60	
Middletemporal	0.78	0.60	
Caudalanteriorcingulate	0.78	0.60	
Insula	0.78	0.59	
Parsopercularis	0.79	0.57	
Superiorfrontal	0.79	0.56	
Transversetemporal	0.81	0.51	
Precentral	0.81	0.50	0.31
Caudalmiddlefrontal	0.81	0.49	0.31
Bankssts	0.81	0.48	0.32
Posteriorcingulate	0.81	0.45	0.37
Supramarginal	0.82	0.43	0.38
Postcentral	0.82	0.40	0.41
Isthmuscingulate	0.78	0.31	0.47
Paracentral	0.81	0.31	0.50
Inferiorparietal	0.80		0.53
Lingual	0.78		0.55
Precuneus	0.78		0.59
Lateraloccipital	0.77		0.62
Superiorparietal	0.74		0.67
Cuneus	0.61		0.78
Pericalcarine			0.38

Note. Loadings for ROI volumes (average of left and right); values <0.3 not shown. General factor loadings of F1 and F2 on *g* were constrained to equality, F1 ~ F2 $r = 0.501$. The S-L transform takes a factor or PC solution, transforms it to an oblique solution, factors the oblique solution to find a higher order (*g*) factor, and then residualizes *g* out of the group factors.

Supplementary Table 6. Comparisons of factor structure of ROI slopes and intercepts (left and right averaged volumes) identified by the exploratory Schmid-Leiman analysis.

		LOADINGS	
Correspondence	**General Factor**	**Factor 1**	**Factor 2**
SLOPES versus INTERCEPTS			
Pearson's *r*	0.30	0.53	0.54
Factor Congruence	0.95	0.88	0.60

Supplementary Table 7. Comparison of Schmid-Leiman factor loadings of bilateral cortical volumes in the main sample and the dementia/MMSE sensitivity sample.

Correspondence	**General Factor**	**Factor 1**	**Factor 2**
SLOPES vs SLOPES			
Pearson's *r*	>0.99	0.98	0.96
Factor Congruence	1.00	1.00	1.00
INTERCEPTS versus INTERCEPTS			
Pearson's *r*	0.92	0.71	0.92
Factor Congruence	1.00	1.00	1.00

Note. Sensitivity sample removed individuals with a self-reported diagnosis of dementia at any wave or a score of MMSE <24. See also Supplementary Figure 5.

Supplementary Table 8. Comparison of Schmid-Leiman factor loadings of bilateral cortical volumes in the main sample and the stroke sensitivity sample.

Correspondence	**General Factor**	**Factor 1**	**Factor 2**
SLOPES vs SLOPES			
Pearson's *r*	0.91	0.82	0.77
Factor Congruence	1.00	0.92	0.84
INTERCEPTS versus INTERCEPTS			
Pearson's *r*	0.95	0.90	>0.99
Factor Congruence	1.00	1.00	1.00

Note. Sensitivity sample removed individuals with stroke at any wave. See also Supplementary Figure 6. Unique participants in the whole sample with a stroke at any wave was N = 119, this equated to a removal of N = 108, N = 64 and N = 48 participants with QC'd FreeSurfer data at Waves 2, 3 & 4, respectively (i.e. many with stroke attended >1 wave).

Supplementary Table 9. Loadings from a confirmatory factor analysis of ROI growth curves.

Region of Interest	*g*	F1	F2
Lateralorbitofrontal	0.39	0.92	
Temporalpole	0.52	0.81	
Frontalpole	0.65	0.76	
Parsorbitalis	0.48	0.70	
Medialorbitofrontal	0.82	0.57	
Fusiform	0.83	0.56	
Parahippocampal	0.67	0.54	
Rostralmiddlefrontal	0.81	0.51	
Inferiortemporal	0.78	0.51	
Middletemporal	0.89	0.48	
Superiortemporal	0.88	0.47	
Entorhinal	0.45	0.46	
Parstriangularis	0.90	0.45	
Rostralanteriorcingulate	0.79	0.42	
Insula	0.92	0.39	
Superiorfrontal	0.97	0.26	
Transversetemporal	0.97	0.25	
Caudalanteriorcingulate	0.98	0.22	
Parsopercularis	0.84	0.22	
Caudalmiddlefrontal	0.97	0.17	0.08
Postcentral	0.76	0.15	0.31
Precentral	0.96	0.14	0.14
Bankssts	0.79	0.13	
Posteriorcingulate	1.00		
Supramarginal	0.94		0.08
Paracentral	0.92		0.39
Isthmuscingulate	0.91		
Inferiorparietal	0.91		0.42
Precuneus	0.87		0.44
Lingual	0.80		0.26
Lateraloccipital	0.77		0.42
Superiorparietal	0.52		0.72
Cuneus	0.35		0.89
Pericalcarine			

Note. Standardised factor loadings reported. Confirmatory factor analysis imposed the factor loading pattern identified from the exploratory analysis, but freely estimated loading magnitudes. Loadings of the paracentral, posterior cingulate and isthmus cingulate were initially found to load on the Schmid-Leiman Factor 1, but were non-significant in the CFA, and so were set to zero.

Supplementary Table 10. Model fit indices for CFAs for cognitive and cortical growth curves (separate measurement models).

	RMSEA	CFI	TLI	SRMR
Cortical ROIs	0.045	0.936	0.921	0.029
g	0.037	0.957	0.955	0.066
Visuospatial	0.036	0.931	0.918	0.048
Processing Speed	0.034	0.924	0.910	0.054
Memory	0.037	0.934	0.921	0.050

Note. RMSEA: root mean squared error of approximation, CFI: comparative fit index, TLI: Tucker Lewis Index, SRMR: standardized root mean square residual.

Supplementary Table 11. Model fit indices for bifactor growth curve SEMs between cortical volumes, *APOE*, and cognitive functions.

	RMSEA	CFI	TLI	SRMR
APOE status	0.035	0.937	0.923	0.029
g	0.030	0.929	0.920	0.048
Visuospatial	0.036	0.931	0.918	0.048
Processing Speed	0.034	0.923	0.909	0.054
Memory	0.037	0.933	0.920	0.050

Note. RMSEA: root mean squared error of approximation, CFI: comparative fit index, TLI: Tucker Lewis Index, SRMR: standardized root mean square residual.

Supplementary Figure 1. Cortical regions of interest.

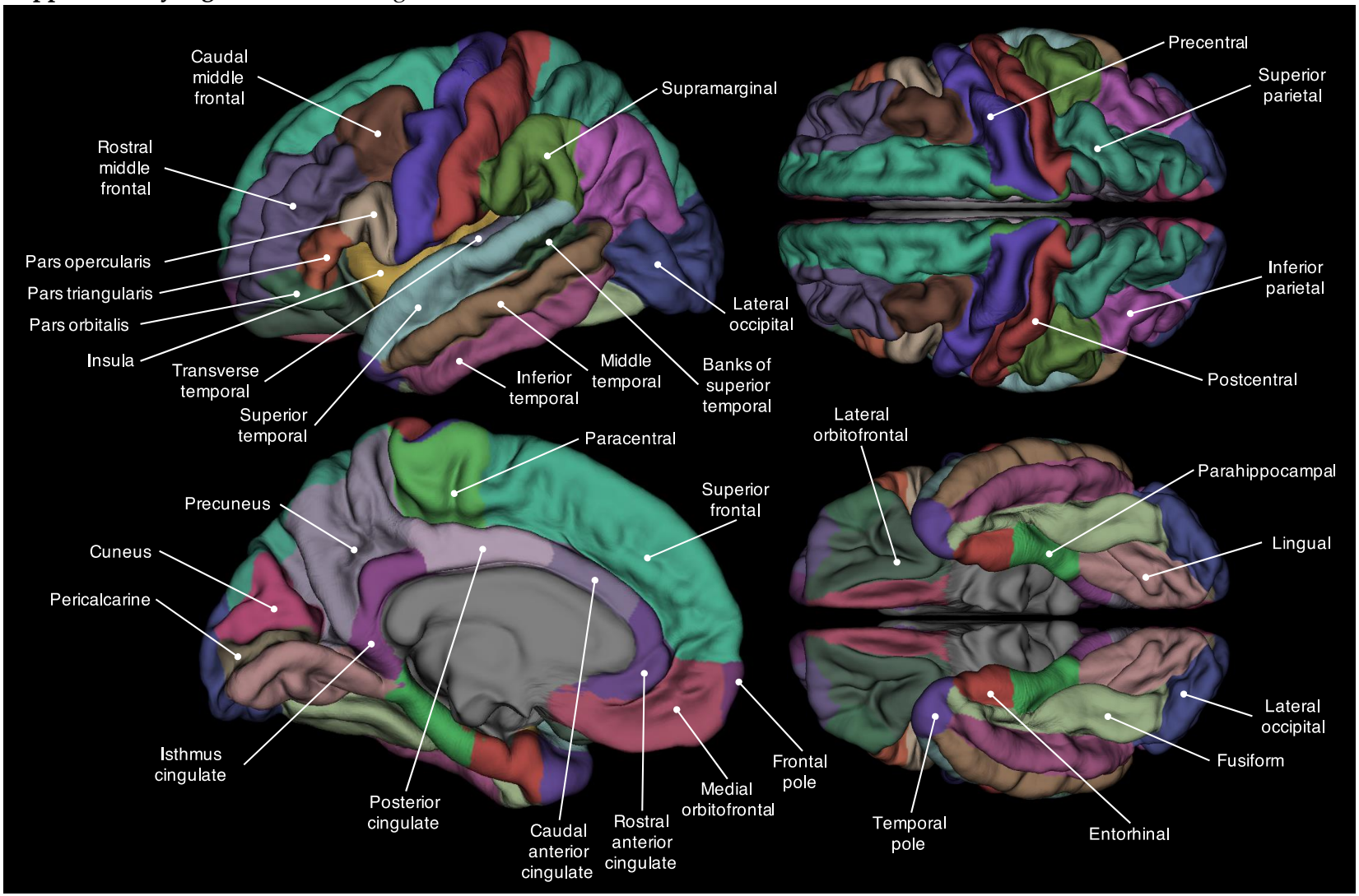

Note. Volumetric parcellation scheme used to identify regions of interest, according to the Desikan-Killiany atlas (Desikan et al., 2006).

Supplementary Figure 2.

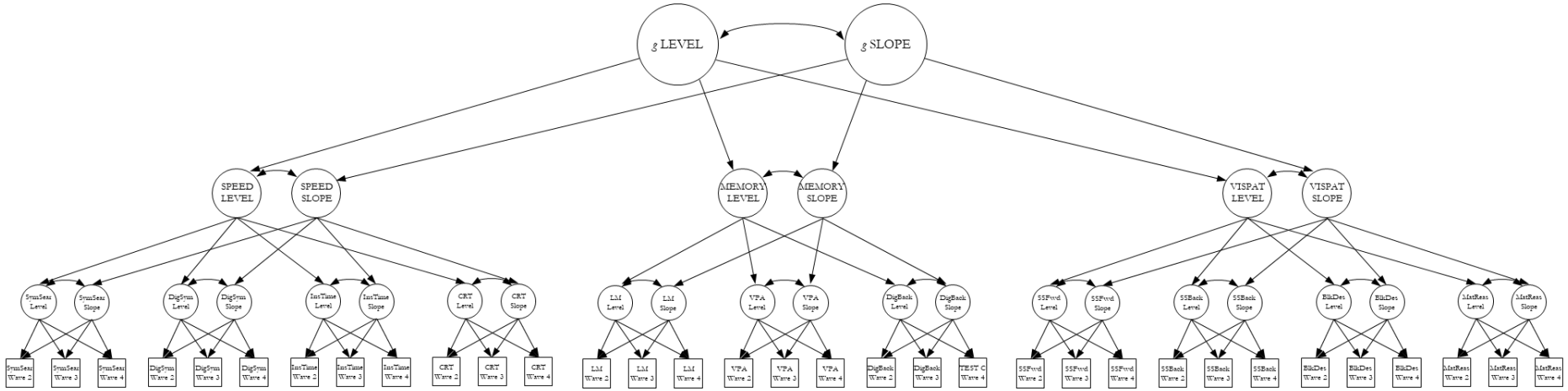

Note. Representation of a latent growth curve analysis in a hierarchical model of cognitive functioning. Manifest variables (i.e. measured test scores) are shown as squares, latent variables are shown as ellipses. The levels and slopes of the cognitive domains of processing speed (SPEED), memory and visuospatial ability (VISPAT) are indicated by the latent levels and changes of measured cognitive test scores across time. A superordinate latent measure of general cognitive ability ('*g*') accounts for the fact that the levels and changes across cognitive test scores in different domains are all positively correlated.

Supplementary Figure 3. Changes in regional cortical volume across the 8th decade, by hemisphere.

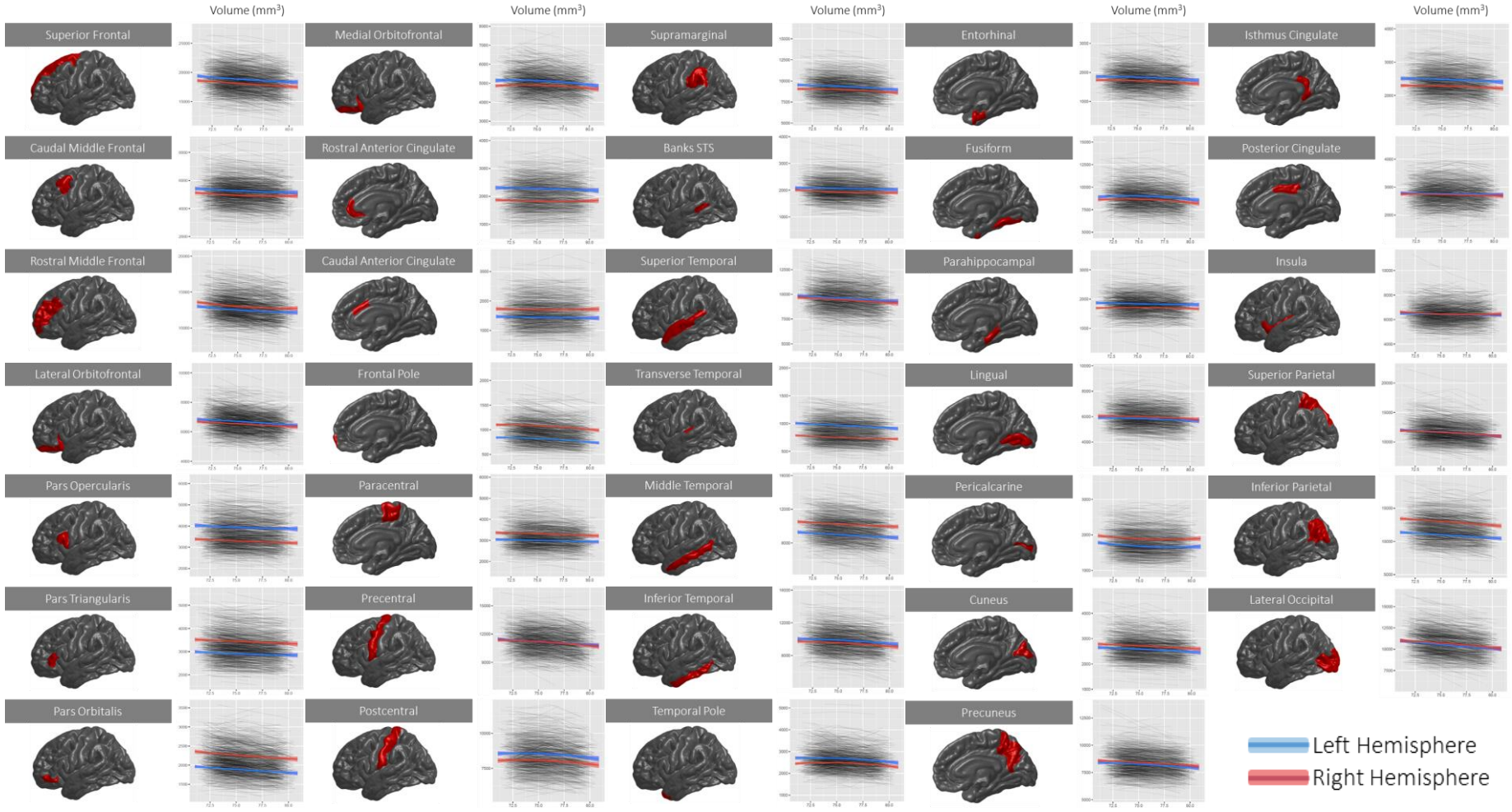

Note. Regional volumes (y-axis; mm³) are shown as age trajectories (x-axis; years) for each participant at each region of interest. Regression lines allowing a quadratic term, with 95% confidence intervals are shown for left and right hemispheres (blue and red, respectively). Unstandardised coefficients are reported in Supplementary Table 1.

Supplementary Figure 4. Correlation matrices and density plots of freely-estimated regional intercepts and slopes; left and right hemisphere comparison.

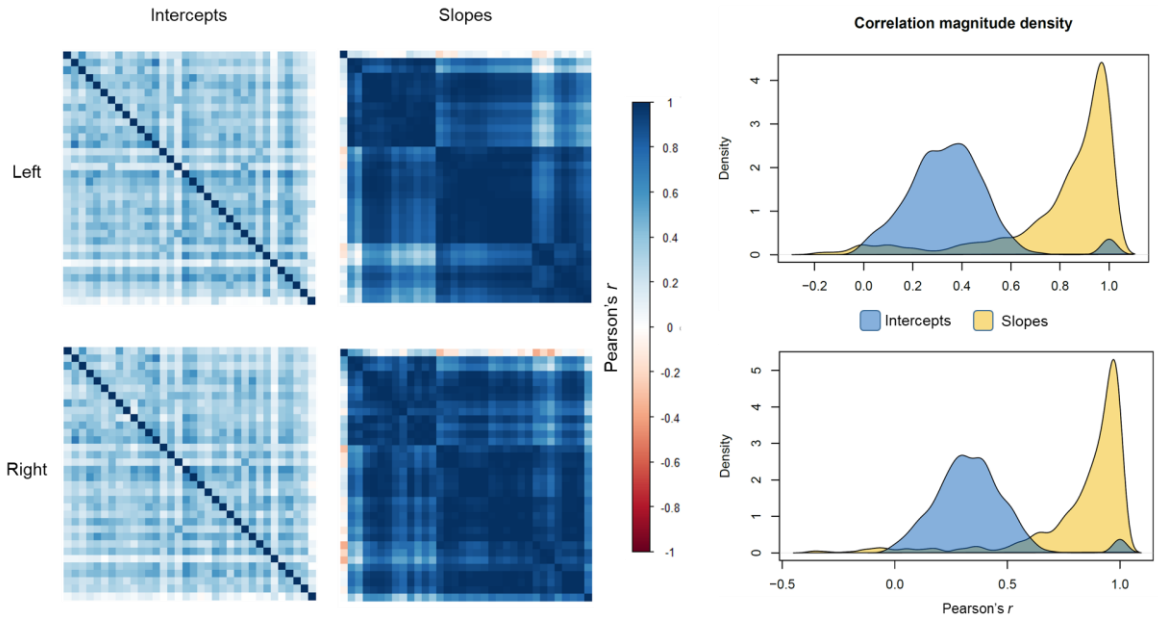

Note. To aid visual comparison of patterns across heatmaps, axes are fixed across matrices.

Supplementary Figure 5. Sensitivity analysis: difference in correlation magnitudes among intercepts and slopes of bilateral regional volumes before and after removing those with dementia or MMSE<24.

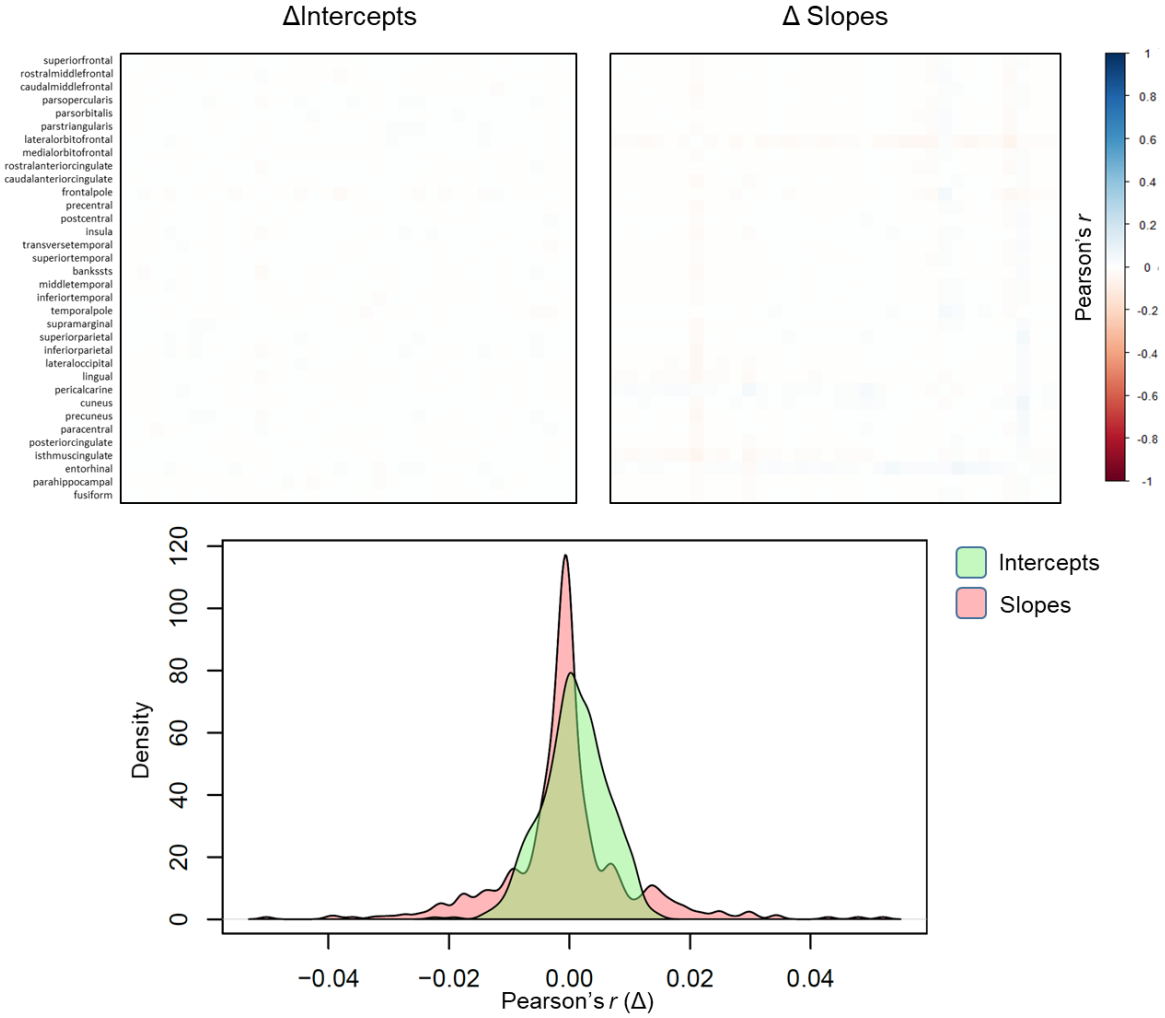

Note. Raw differences (Δ) between correlation magnitudes are shown for intercepts and slopes (top). The density plot shows the Δ distributions. Alongside the similarity of the resultant factor structure (see Supplementary Table 7), these results indicate that possible dementia cases are unlikely to have been driving the observed ageing patterns.

Supplementary Figure 6. Sensitivity analysis: difference in correlation magnitudes among intercepts and slopes of bilateral regional volumes before and after removing those with stroke.

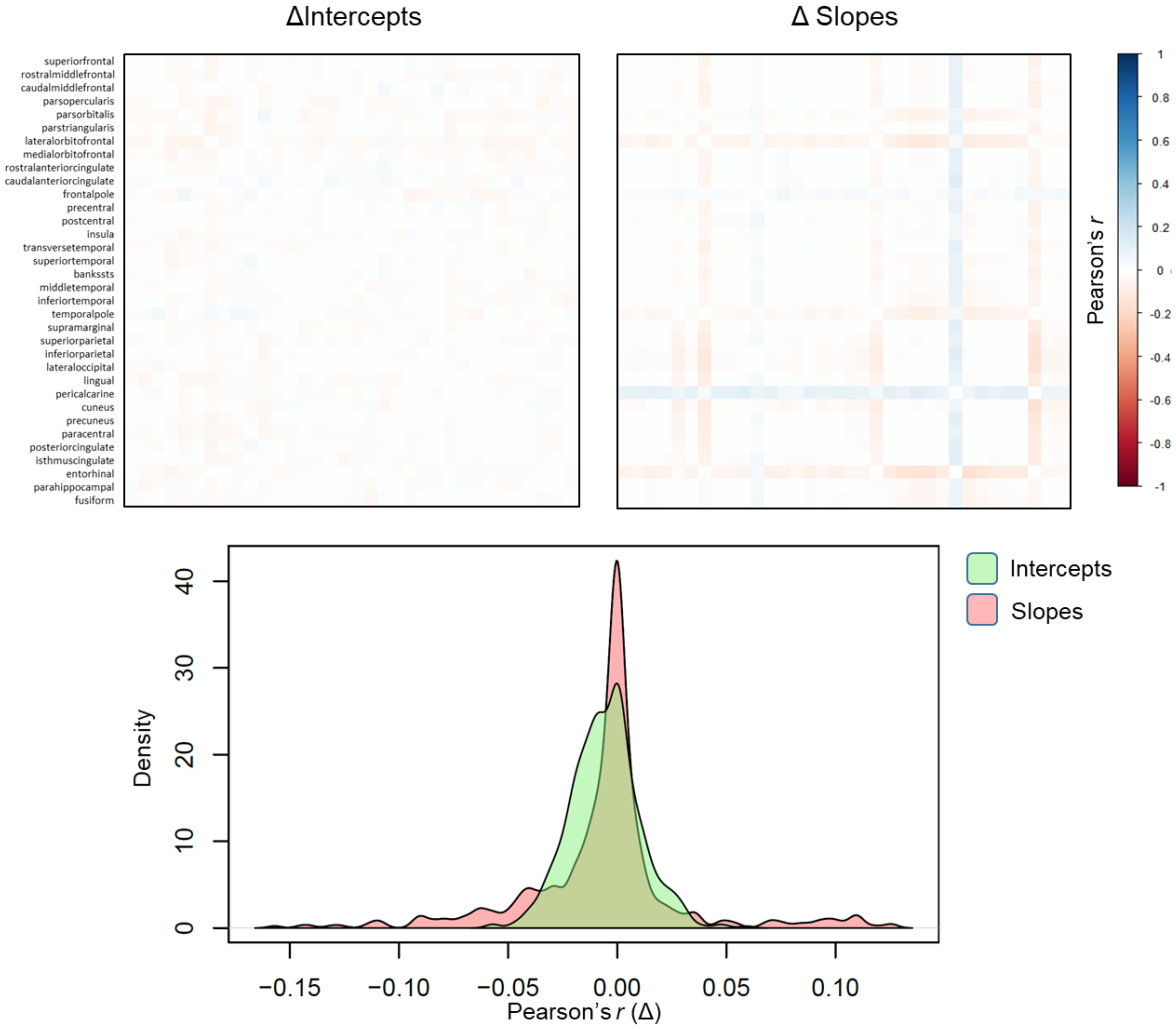

Note. Raw differences (Δ) between correlation magnitudes are shown for intercepts and slopes (top). The density plot shows the Δ distributions. Alongside the similarity of the resultant factor structure (see Supplementary Table 8), these results indicate that stroke cases are unlikely to have been driving the observed ageing patterns.

Supplementary Figure 7. Correspondence between standardised loadings for factors of cortical change estimated via exploratory and confirmatory factor analyses.

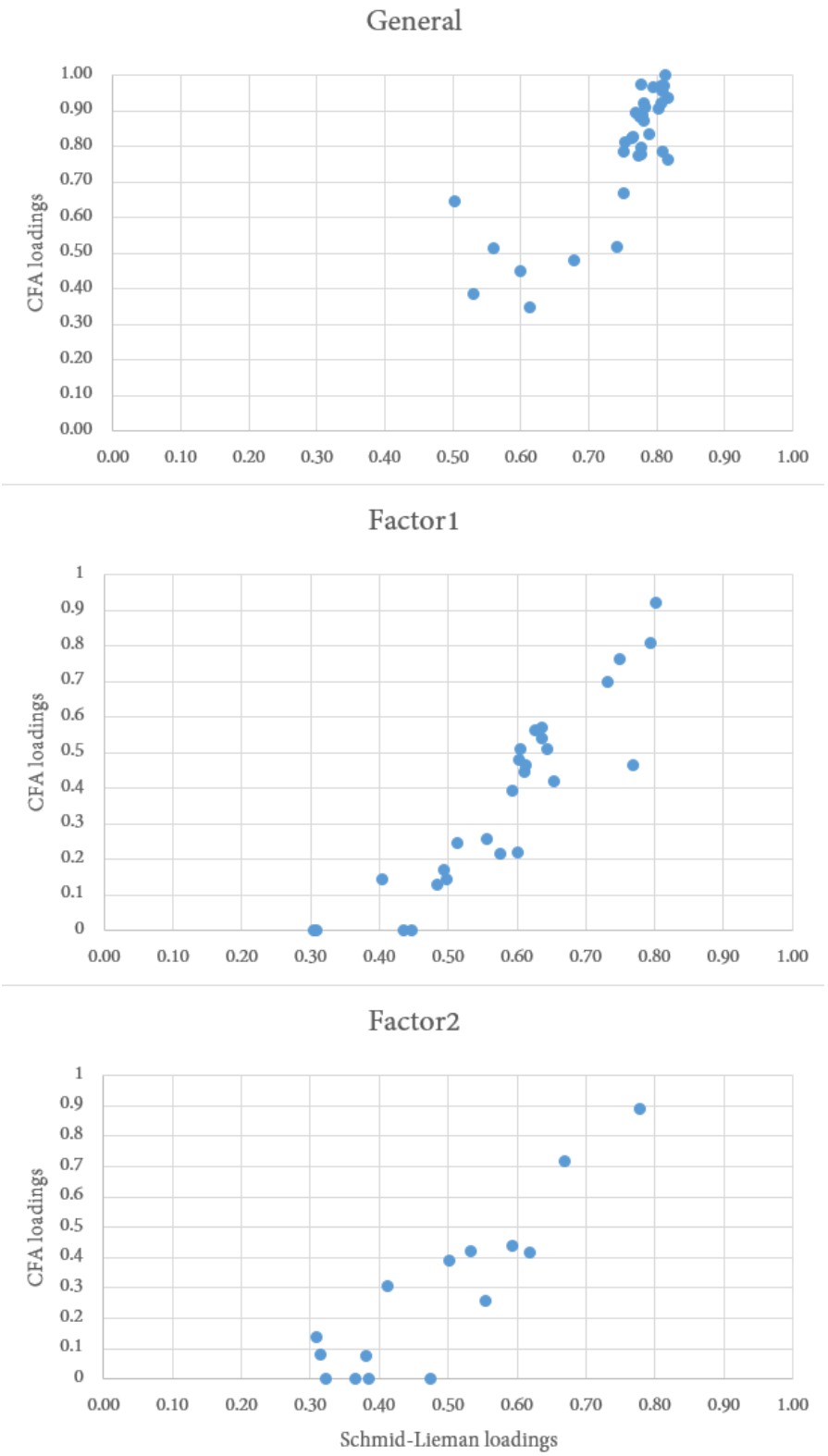

Note. X and Y axes denote standardised factor loadings from the exploratory Schmid-Leiman (X) and CFA (Y). Correlations (Pearson's *r*) between EFA and CFA loadings for each factor were: General = 0.856, Factor 1 = 0.831, Factor 2 = 0.826.